

Matthew Ndubuisi ABONYI¹ 

Joseph Tagbo NWABANNE¹

Samuel Chigozie NZEKWE¹

Clinton Chizoba ELE¹

Blessing Chiemerie ORUNTA¹

Lawrence Ifeanyi IGBONEKWU²

¹ Nnamdi Azikiwe University, Faculty of Engineering, Department of Chemical Engineering, Nigeria

² Nnamdi Azikiwe University, Faculty of Engineering, Department of Petroleum Engineering, Nigeria

Adsorptive removal of a nitrate ion from the aqueous solution of sodium nitrate by application of double fixed-bed column

Keywords: nitrate, rice husk, fixed-bed, double parking, adsorption

Introduction

One of the prominent global challenges in water pollution of the environment involves the contamination caused by nitrogen-containing compounds such as nitrate, nitrite, and ammonium (Ward et al., 2018). Groundwater can be susceptible to nitrate ion contamination due to excessive fertilizer usage in agriculture (El Ouardi et al., 2015; Jiaa et al., 2020). Nitrate salts, including potassium nitrate, sodium nitrate, calcium nitrates, and ammonium, find applications in the manufacturing of nitrogen-based fertilizers, specialized cement formulation, as food additives and

dyes (Daouda et al., 2018). The World Health Organization has established daily maximum acceptable limits for nitrate at 0.3–0.7 mg·kg⁻¹. The maximum acceptable limit of nitrate in water for human consumption is set at 50 mg·l⁻¹ (World Health Organization [WHO], 2017). Nitrate contamination poses risks to human health primarily through the conversion of nitrates to nitrites, which are highly soluble in aqueous solutions and pose threats to drinking water supplies and promote eutrophication in groundwater (El Ouardi et al., 2015).

The reduction of nitrate to nitrosamines in the stomach can lead to various health problems such as prostate, pharynx, esophagus, or colon cancer (Zheng & Wang, 2010). In infants, the conversion of nitrate to nitrite, which later reacts with hemoglobin, can cause methemoglobinemia or blue baby syndrome, resulting in blueness of the skin in newborn babies (El Ouardi et al., 2015). Nitrate-contaminated water bodies have been known to contribute to infectious diseases in humans (El Ouardi et al., 2015). Furthermore, high concentrations of nitrate in aqueous solutions have been associated with miscarriages, eutrophication, harmful algal proliferation, hypoxia, and loss of biodiversity (Tejada-Tovar et al., 2021). Consequently, there is a pressing need to reduce nitrate levels in water to meet acceptable standards.

Various techniques have been employed to remove nitrate from aqueous solutions, including electrodialysis (Koter et al., 2015), adsorption (Tong et al., 2017; Taoufik et al., 2020), biological methods (Shi et al., 2013; Li et al., 2017), ion exchange (Werth et al., 2021), reverse osmosis (Shelly et al., 2021), nano-filtration membrane (Adeniyi et al., 2022), freeze-melting (Hosseini & Mahvi, 2018), chemical reduction (El Ouardi et al., 2015), coagulation, oxidation, precipitation, and filtration (Kumar et al., 2010; Foo & Hameed, 2012). However, many of these techniques are expensive and not economically feasible for large-scale industries. Additionally, some methods result in the generation of secondary pollutants, such as residues of dead bacteria from biological approaches, which can pose challenges in subsequent processes. Therefore, there is a need to explore simple, cost-effective, efficient, and environmentally friendly techniques, such as adsorption onto micro-porous solids like activated carbon (Varsha et al., 2022).

In recent years, several adsorbents have been utilized to remove contaminants, particularly nitrate, from aqueous solutions. These include nanoparticles (Tyagi et al., 2018), modified chitosan beads (Jamka & Mohammed, 2023), local clay (Battas et al., 2019), organic resin (Li et al., 2020), mineral-based adsorbents (Chen et al., 2020), and nanostructured carbon (Liu et al., 2018). However, many of these adsorbents are expensive, non-biodegradable, and require complicated synthesis processes (Quang et al., 2022). Therefore, it is crucial to develop adsorbents

through simple synthesis methods to reduce costs. Activated rice husk presents itself as a favorable alternative due to its affordability, availability, and excellent adsorption properties.

The study of nitrate adsorption in packed columns has gained significant interest. Consequently, conducting column studies is essential to determine the necessary contact time for achieving adsorbate equilibrium. Column adsorption studies hold significance for industrial applications since findings from batch adsorption studies may not be directly applicable to field applications in treating contaminated water (Jahangiri-Rad et al., 2014). Fixed column adsorption proves to be a better, simpler, and more economical method for removing various contaminants industrially. Moreover, fixed bed columns are preferable over batch adsorption because they offer industrial feasibility for removing various contaminants from either real wastewater or synthetic effluent. Literature reveals numerous studies focused on single-packed column adsorption of nitrate from aqueous solutions, but none have explored the impact of multiple parking in a column. Introducing multiple parking in a column or utilizing serially connected columns could enhance the efficiency of the adsorption process, thereby justifying the need for this study. This research utilizes activated rice husk carbon in a double-parked fixed adsorption column to remove nitrate from aqueous solutions. The study investigates the influence of parking height, flow rate variation, adsorbate concentration, and the number of parking layers on the adsorptive removal of nitrate from aqueous solutions.

Material and methods

Adsorbent (rice husk activated carbon) preparation

The rice husk was obtained from Mgbakwu, Awka North in Anambra State, Nigeria (6°16'20" N and 7°3'21" E). It underwent a series of preparation steps for the experimental use. Initially, it was carefully sorted to eliminate any impurities, followed by thorough washing with clean tap water. The husk was then dried in sunlight until it reached a moisture-free state. Subsequently, the rice husk underwent thermal carbonization at 450°C in a gas oven, maintaining this temperature for a duration of 30 min. After the carbonization process, the material was allowed to cool down to room temperature and stored in an air-tight container for further use. Before being utilized, the rice husk was manually crushed and sieved to achieve a particle size of 300 µm, suitable for the experimentation. The carbonized rice husk fibers were impregnated with 1M H₂SO₄ for a 24 h,

followed by heating at 700°C with a heating rate of 10°C·min⁻¹ for a period of 2.3 h. Subsequently, the samples were removed, cooled, and thoroughly washed with deionized water multiple times to eliminate any residual acid from the H₂SO₄ treatment. The pH of the material was monitored using litmus paper until it reached a neutral state. Finally, the adsorbent was dried in an oven at 105°C for 60 min and underwent separation into different sizes using a mechanical shaker.

Nitrate solution preparation

To prepare the stock solution, a 1.0 g of sodium nitrate salt was dissolved in 200 ml of distilled water in a 1,000 ml volumetric flask and shaken to dissolve. It was thereafter made up to the mark with distilled water. The stock solution was serially diluted to obtain various concentrations ranging from 100 mg·l⁻¹, 150 mg·l⁻¹ and 200 mg·l⁻¹ of nitrate solution for the experiment.

Characterization of the rice husk activated carbon

The functional groups present in the samples were determined by the Fourier transform infrared machine, Cary 630 model, with Agilent technology. The adsorbent's chemical compositions were determined by X-ray fluorescence. While the surface morphology of the samples were determined by a scanning electron microscope (SEM) coupled with energy-dispersive spectroscopy (EDS) of model JOEL-JSM 7600F.

Packed bed adsorption apparatus set up

The experimental setup for the packed bed column consisted of a plastic column measuring 60 cm in height and 0.9 cm in diameter (refer to Fig. 1). To secure the packing material in place and prevent the passage of activated rice husk carbon (RHAC) particles, a wire mesh and cotton wool were placed at the bottom of each packing layer. The column was clamped to a stand, and a small hose connected to a peristaltic pump was used to introduce the nitrate solution from a beaker at a flow rate of 20 ml·min⁻¹ into the top of the column.

To maintain consistent flow conditions and prevent changes in the nitrate solution flow rate upon entering the second packing layer, the entire adsorption experiment was conducted with the direction of flow from the top to the bottom of the column. Residual nitrate solution samples were collected at the sample point

located at the side of the column using a syringe for the first packing layer. For the second packing layer, the residual nitrate solution was collected at the bottom of the column using a beaker.

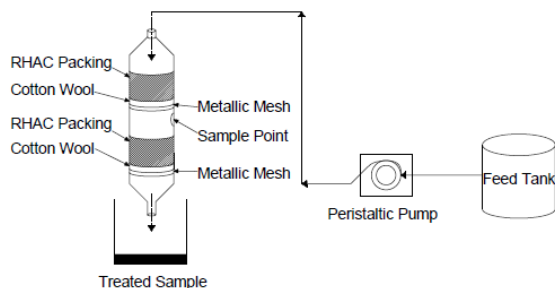


FIGURE 1. Double packed fixed bed adsorption column

Source: own work.

Finally, the initial concentration of the nitrate solution and the concentration of the nitrate solution samples obtained from both stages were analyzed using a UV spectrophotometer to determine the concentration of nitrate ions in the effluent sample.

Column experiment

Column experiment was performed to evaluate the effect of nitrate solution flow rate, number of packing, height of adsorbent packing and initial nitrate solution concentration on adsorption performance of RHAC and each of the experiment was performed as follows.

Effect of initial nitrate solution concentration

To investigate the impact of initial concentration on the adsorption performance of activated rice husk carbon (RHAC), nitrate solutions with concentrations of $100 \text{ mg}\cdot\text{l}^{-1}$, $150 \text{ mg}\cdot\text{l}^{-1}$, and $200 \text{ mg}\cdot\text{l}^{-1}$ were prepared from the stock solution. For the initial concentration of $100 \text{ mg}\cdot\text{l}^{-1}$, a 400-milliliter nitrate solution was measured and placed in a 500-milliliter beaker. The peristaltic pump was then utilized to pump the nitrate solution into the adsorption column at a constant flow rate of $10 \text{ ml}\cdot\text{min}^{-1}$. The column maintained a consistent packing height of 5 cm with the RHAC.

Samples were collected at five-minute intervals over a duration of 60 min. Each sample was collected and stored for a subsequent analysis. The analysis involved using a UV spectrophotometer at a wavelength of 220 nm to determine the nitrate ion concentration in the collected samples. This entire procedure was repeated for the initial concentrations of $150 \text{ mg}\cdot\text{l}^{-1}$ and $200 \text{ mg}\cdot\text{l}^{-1}$ of sodium nitrate solution to assess their respective adsorption performances.

Effect of bed height

To examine the impact of the height of adsorbent packing on the adsorptive performance of activated rice husk carbon (RHAC), three different packing heights were considered: 3 cm, 5 cm, and 7 cm. Throughout the experiment, a peristaltic pump was employed to transfer the nitrate solution from a beaker into the packed column. The initial concentration of the nitrate solution, flow rate, and the number of packing remained constant at $100 \text{ mg}\cdot\text{l}^{-1}$, $10 \text{ ml}\cdot\text{min}^{-1}$, and single packing, respectively.

At regular intervals of 5 min, samples were collected using sample bottles for each of the three different packing heights (3 cm, 5 cm, and 7 cm) over a total duration of 60 min. The collected samples were then analyzed using a UV-visible spectrophotometer at a wavelength of 220 nm to determine the concentrations of the samples.

Effect of number of rice activated carbon packing

To investigate the influence of the number of packing on the adsorption performance of RHAC, an adsorption column was constructed with two packings of RHAC, each 5 cm high. A 400-milliliter nitrate solution with a constant concentration of $100 \text{ mg}\cdot\text{l}^{-1}$ was measured using a measuring cylinder and placed in a beaker.

Using a peristaltic pump, the nitrate solution was continuously pumped into the adsorption column at a consistent flow rate of $10 \text{ ml}\cdot\text{min}^{-1}$. Samples were collected at two points within the column: below the first packing and at the exit bottom end. The collection of samples began at an initial time of 5 min and continued until 60 min. After the collection of samples, the nitrate ion concentration in each sample was determined using a UV spectrophotometer at a wavelength of 220 nm.

Adsorption modeling

Three adsorption modelling were employed to fit the data and describe the adsorption performance of the column. The models are Adams–Bohart, Thomas and Yoon–Nelson models. The non-linear and linear model used in this study are presented in Table 1.

TABLE 1. List of column adsorption models used

Model	Non-linear	Linear	Plot made	Eq.	Reference
Thomas	$\frac{C_t}{C_o} = \frac{1}{1 + \exp\left(\frac{K_{Th} q_o x}{Q} (q_t x - C_o v_{eff})\right)}$	$\ln\left[\frac{C_o}{C_t} - 1\right] = \left[\frac{K_{Th} q_o x}{Q}\right] - K_{Th} C_o t$	$\ln\left[\frac{C_o}{C_t} - 1\right] \text{ vs } t$	(1)	Swarup & Umesh, 2015
Adams–Bohart	$T = \left[\frac{N_o z}{C_o v}\right] \left[\frac{\ln\left(\frac{C_o}{C_t} - 1\right)}{C_o K_{AB}}\right]$	$\ln\left(\frac{C_t}{C_o}\right) = K_{AB} C_o t - \frac{K_{AB} N_o Z}{F}$	$\ln\left(\frac{C_t}{C_o}\right) \text{ vs } t$	(2)	Swarup & Umesh, 2015
Yoon–Nelson	$\frac{C_t}{C_o} = \frac{1}{1 + e^{K_{YN}(t-\tau)}}$	$\ln\left(\frac{C_t}{C_o - C_t}\right) = K_{YN} t - \tau K_{YN}$	$\ln\left(\frac{C_t}{C_o - C_t}\right) \text{ vs } t$	(3)	Chen et al., 2017

Note: C_o – initial concentration, C_t – concentration at time (t), K_{Th} – Thomas rate constant [$l \cdot mg^{-1} \cdot min^{-1}$], Q – flow rate [$ml \cdot min^{-1}$], q_t – nitrate uptake per 1 g of the adsorbent at time (t) [$mg \cdot g^{-1}$], x – mass of the used adsorbent [g], v_{eff} – the effluent volume [ml], q_o – maximum nitrate uptake per 1 g of the adsorbent [$mg \cdot g^{-1}$], T – the time required for 50% adsorbate breakthrough [min], N_o – saturation concentration [$mg \cdot l^{-1}$], Z – bed height of column [cm], v – volume [ml], K_{AB} – the kinetic constant for the Adams–Bohart model [$l \cdot mg^{-1} \cdot min^{-1}$], F – superficial velocity calculated by dividing the flow rate by the column section area [$cm \cdot min^{-1}$], e – exponent, K_{YN} – Yoon–Nelson rate constant [min^{-1}], τ – breakthrough time required for 50% adsorbate breakthrough [min].

Source: own work.

Results and discussion

Fourier transformed infrared (FTIR)

The Fourier transform infrared (FTIR) analysis of both rice husk biomass (RHB) and rice husk activated carbon (RHAC) samples was conducted within the wave number range of 500 cm^{-1} to $4,000 \text{ cm}^{-1}$. The results are presented in Table 2. Several significant absorption peaks were observed in the RHB sample. Notably, large absorption peaks were observed at $3,898.8 \text{ cm}^{-1}$, $3,749.7 \text{ cm}^{-1}$, and $3,313.6 \text{ cm}^{-1}$, which can be attributed to the overlapping stretching vibrations of hydroxyl (OH) and amino (NH_2) groups present in pure rice husk (Abonyi et al., 2023). The peak at $3,749.6 \text{ cm}^{-1}$ corresponds to the Si-OH stretching vibration

of rice husk. Additionally, characteristic peaks of carbonyl group stretching for aldehydes and ketones were observed at $1,897.2\text{ cm}^{-1}$ and $1,695.9\text{ cm}^{-1}$, respectively. The band at $1,568.0\text{ cm}^{-1}$ indicates the presence of the COO-group, which can be attributed to the H_2SO_4 used during the activation process of the rice husk. The peak at $2,322.1\text{ cm}^{-1}$ corresponds to the stretching vibration of Si-H, while the bands in the $1,058.6\text{ cm}^{-1}$ region represent the stretching vibration of Si-O. The stretching vibrations of $-\text{NH}_2$ groups were detected at 898.3 cm^{-1} .

Upon adsorption of sodium nitrate by the activated rice husk (RHA), changes in the peaks of certain functional groups were observed. Some functional groups, such as the ones at $3,898.8\text{ cm}^{-1}$, $3,749.7\text{ cm}^{-1}$, $3,313.6\text{ cm}^{-1}$, $2,616.6\text{ cm}^{-1}$, $2,448.9\text{ cm}^{-1}$, $2,322.1\text{ cm}^{-1}$, and $1,695.9\text{ cm}^{-1}$, completely disappeared. Simultaneously, new functional groups emerged, as evidenced by the appearance of peaks at $3,268.9\text{ cm}^{-1}$, $2,918.5\text{ cm}^{-1}$, and $1,222.6\text{ cm}^{-1}$. These changes indicate the adsorption of nitrate onto the surface of the activated rice husk (RHA), resulting in the alteration of certain functional groups and the formation of new ones.

TABLE 2. FTIR spectral of RHA and RHB

s/n	Wave number of RHB [cm ⁻¹]	Wave number of RHA [cm ⁻¹]	Difference in wave number [cm ⁻¹]	Functional group
1	3 898.8	disappeared	3 898.8	alkane
2	3 749.7	disappeared	3 749.7	Si-OH
3	3 313.6	disappeared	3 313.6	-OH
4	absent	3 268.9	3 268.9	-O-H
5	absent	2 918.5	2 918.5	C-H
6	2 616.6	disappeared	2 616.6	N-H stretching
7	2 448.9	disappeared	2 448.9	C≡C stretching
8	2 322.1	disappeared	2 322.1	Si-H
9	2 042.4	2 109.7	66.6	-C≡C-
10	1 897.2	1 990.4	93.2	aldehyde
11	1 695.9	disappeared	1 695.9	ketone
12	1 568.0	1 576.7	8.7	COO-
13	absent	1 222.6	1 222.6	C-N
14	1 058.6	1 095.8	37.2	Si-O
14	782.7	898.3	115.6	-NH ₂

Source: own work.

Scanning electron microscopy (SEM-EDS)

The surface description and composition of the rice husk samples were analyzed using SEM-EDS (scanning electron microscopy-energy dispersive X-ray spectroscopy). Figure 2a shows the SEM micrograph of the untreated rice husk biomass (RHBS). It reveals that the sample exists in an amorphous silica form. Upon closer examination, the micrograph exhibits longitudinal-like fibrous particles of rice husk. Spaces and cavities are observed throughout the micrograph, which may aid in the adsorption of metals and ions in different areas of the material. These surface features indicate the potential of RHBS to retain nitrate ions.

Figure 3a depicts the SEM micrograph of the activated rice husk (RHAC). Compared to RHB in Figure 2a, the surface of RHAC shows fewer and less developed pores, as well as a less ordered and fewer flake-like structure. This variation in surface morphology between RHB and RHAC can be attributed to the adsorption of nitrate ions into the pores of the adsorbent. Thus, the observed morphologies in RHBS and RHAC present favorable surface characteristics for nitrate ion retention.

The compositions of the samples were determined using SEM-EDS, and the results are presented in Figures 2b and 3b. According to Figure 2b, RHBS primarily consists of silica (42.20%), oxygen (35.30%), and calcium (12.33%). Other components present in RHBS include carbon (5%), potassium (2.17%), and magnesium (1.25%). In Figure 3b, a larger percentage of RHAC is composed of calcium (12.33%), oxygen (20.30%), and silica (52.20%). The remaining components in RHAC are the same as in RHBS, except for the introduction of aluminum (6.30%) in RHAC.

Comparing Figures 2b and 3b, the EDS analysis reveals changes in the elemental composition of the activated rice husk after adsorption. There is a significant

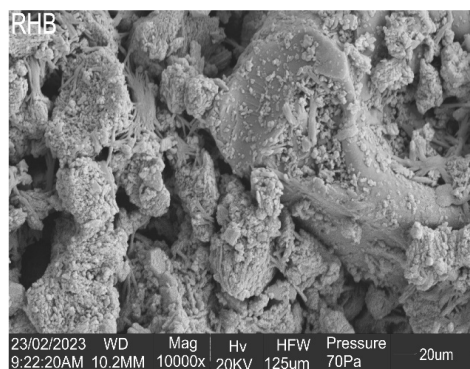


FIGURE 2a. SEM image of RHBS

Source: own work.

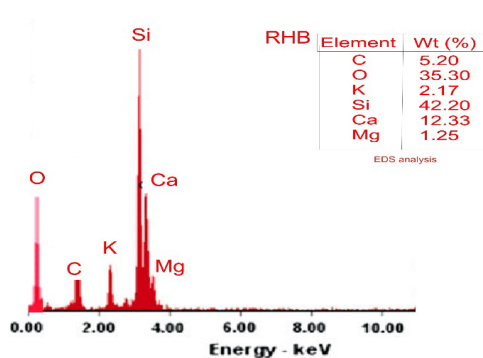


FIGURE 2b. EDS of RHBS

Source: own work.

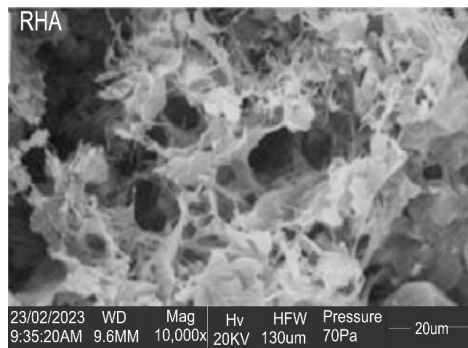


FIGURE 3a. SEM image of RHAC
Source: own work.

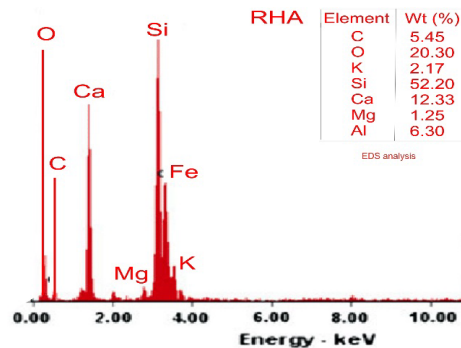


FIGURE 3b. EDS of RHAC
Source: own work.

decrease in the weight percentage [wt%] of oxygen and the introduction of aluminum (Al), which likely originated from impurities present in the nitrate salt solution used. The decrease in oxygen can be attributed to the adsorption of nitrate ions onto the surface of the activated rice husk. The increase in aluminum may be attributed to the formation of aluminum oxide or aluminum hydroxide complexes during the adsorption process. Notably, there is an increase in the weight percentage of silicon (Si) after adsorption, indicating that the adsorption process did not significantly remove Si from the activated rice husk. This is important as Si is a crucial component of the activated rice husk structure, and its removal could affect the porosity and surface area of the adsorbent. The highest peak obtained for Si occurred at 3.7 keV. The presence of potassium (K) and magnesium (Mg) before and after adsorption suggests that these elements are not significantly affected by the adsorption process and may play a lesser role in nitrate ion adsorption.

XRF analysis of rice husk

The X-ray fluorescence (XRF) analysis results for RHA and RHB are presented in Tables 3 and 4. Table 3 indicates that SiO_2 , P_2O_5 , CaO , and K_2O are the predominant oxides in both RHAC and RHBS. SiO_2 has the highest concentration in both RHA (71.315%) and RHBS (74.476%). It is notable that RHAC shows an increase in the concentration of SiO_2 , CaO , and Al_2O_3 compared to RHBS. On the other hand, RHAC exhibits decreased concentrations of MnO , Fe_2O_3 , P_2O_5 , and K_2O compared to RHBS. Table 4 illustrates the elemental compositions of RHAC and RHBS as determined by the XRF analysis. Each element has characteristic X-ray peaks at different wavelengths, and the fluorescence intensity of each spectral

line corresponds to the element concentration. The results reveal that RHAC has increased relative quantities of oxygen (O), aluminum (Al), silicon (Si), sulfur (S), calcium (Ca), and manganese (Mn), while exhibiting decreased concentrations of phosphorus (P), potassium (K), titanium (Ti), and iron (Fe).

TABLE 3. Concentrations of oxides in rice husk XRF analysis

Major oxides	Concentration [wt%]	
	RHBS	RHACS
SiO ₂	71.315	74.476
MnO	0.826	0.672
Fe ₂ O ₃	0.658	0.510
CuO	0.120	0.121
P ₂ O ₅	7.568	6.560
SO ₃	1.670	1.767
CaO	4.718	5.211
MgO	0.000	0.000
K ₂ O	8.037	5.881
Al ₂ O ₃	1.497	1.744
TiO ₂	0.383	0.161
ZnO	0.081	0.088

Source: own work.

TABLE 4. Concentrations of trace metals in the rice husk XRF analysis

Trace element	Concentration [ppm]	
	RHBS	RHAC
O	47.252	48.153
Al	0.792	0.923
Si	33.336	34.184
P	3.303	2.863
S	0.669	0.708
Cl	3.059	2.713
K	6.672	4.882
Ca	3.372	3.724
Ti	0.230	0.096
Mn	0.640	0.520
Fe	0.460	0.357
Cu	0.096	0.097
Zn	0.065	0.071

Source: own work.

These elemental compositions may influence the adsorption of nitrate ions onto the rice husk surface through ion exchange processes. The increased nitrate ion uptake by RHAC can potentially be attributed to the higher concentrations of more easily exchangeable elements such as Si and K. The XRF analysis provides valuable information regarding the elemental composition of the samples, which is instrumental in understanding the chemical properties of both the rice husk and the aqueous solution. The information obtained from the XRF analysis can be utilized to optimize the process, enhance product quality, and reduce waste.

Effect of initial concentration of nitrate ion on breakthrough curve

The performance of the column was evaluated at initial nitrate ion concentrations of $100 \text{ mg}\cdot\text{l}^{-1}$, $150 \text{ mg}\cdot\text{l}^{-1}$, and $200 \text{ mg}\cdot\text{l}^{-1}$. The bed height and flow rate were kept constant at 7 cm and $8.33\cdot 10^{-8} \text{ m}^3\cdot\text{s}^{-1}$, respectively. The results are depicted in Figure 4.

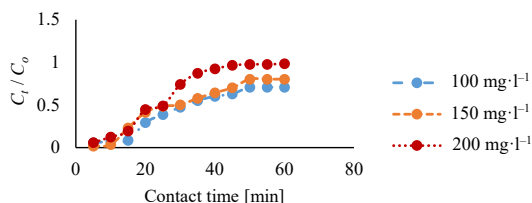


FIGURE 4. Effect of initial nitrate ion solution

Source: own work.

It can be observed that as the initial nitrate ion concentration increased from $100 \text{ mg}\cdot\text{l}^{-1}$ to $200 \text{ mg}\cdot\text{l}^{-1}$, the breakthrough time decreased. This indicates that the adsorption bed became saturated more quickly at higher initial concentrations due to the rapid saturation of binding sites within the column. At $200 \text{ mg}\cdot\text{l}^{-1}$ initial concentration, the column achieved a higher efficiency at saturation, with a value of 96.52%, compared to 70.24% and 62.99% for $150 \text{ mg}\cdot\text{l}^{-1}$ and $100 \text{ mg}\cdot\text{l}^{-1}$, respectively.

The higher efficiency at higher initial concentrations can be attributed to the increased driving force provided by the higher concentration of adsorbate (nitrate ion). This is necessary to overcome the mass transfer resistance between the aqueous solution and the RHAC adsorbent phase. As a result, there is greater collision between the nitrate ions and the active sites of the RHAC, leading to enhanced adsorption.

In summary, the RHAC reached saturation earlier at higher initial concentrations, resulting in a reduced breakthrough time. This can be attributed to the higher initial concentrations of nitrate ions saturating the RHAC more rapidly. Conversely, lower initial concentrations of nitrate ion tend to delay the breakthrough point due to slower transport velocity and longer contact time resulting from a lower concentration gradient. Similar findings have been reported in studies conducted by Swarup and Umesh (2015), and Chen et al. (2017).

Effect of bed height on breakthrough curve

The impact of bed height on the breakthrough curve is illustrated in Figure 5. It can be observed that increasing the bed height from 3 cm to 7 cm resulted in an increase in the breakthrough time. This is because an increase in bed height leads to the addition of more sorption sites, which are necessary for the adsorption of nitrate ions. With a reduced bed height, the nitrate ions have limited time to come into contact with the RHAC surface, resulting in a decreased breakthrough time.

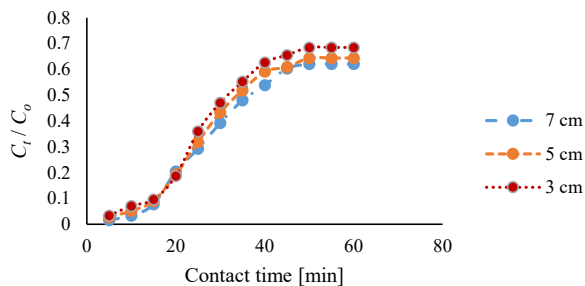


FIGURE 5. Effect of bed height on nitrate ion removal

Source: own work.

The maximum removal of nitrate from the aqueous solution using RHAC occurs in the initial stages of the adsorption process. However, over time, the sorption of nitrate ions decreases due to the depletion of available sorption sites required for nitrate ion removal. In the design and operation of a fixed bed column, a greater bed height and slower exhaustion of the adsorbent bed are desirable as they increase the adsorption capacity while extending the breakthrough time. On the other hand, a reduced bed height does not provide sufficient time for the adsorbate (nitrate ion) to diffuse into the active sites of the RHAC, resulting in a shorter breakthrough time.

Similar trends have been reported in studies conducted by Mondal (2009) and Omitola et al. (2022). They found that increasing the bed height led to an increase in breakthrough time and improved adsorption capacity.

Effect of number of parking in a column on breakthrough curve

The impact of the number of packing (or beds) in the fixed bed column was investigated under constant flow rate ($8.33 \cdot 10^{-8} \text{ m}^3 \cdot \text{s}^{-1}$) and initial concentration ($100 \text{ mg} \cdot \text{l}^{-1}$). The configuration consisted of two packings with a height of 7 cm each, separated by a 10 cm gap, as illustrated in Figure 1. The purpose of introducing multiple packing to the column was to assess the effect of additional beds on the removal efficiency of nitrate ions.

Figure 6 demonstrates that the inclusion of an extra packing or bed tends to enhance the efficiency of the adsorption column. At saturation, the optimal removal efficiency of nitrate ions for the first bed was 60.3%, whereas the introduction of the second fixed bed increased the efficiency to 81.4%. The addition of a fixed bed to the column results in an increased amount or number of sorption sites, as well as an extended service time until breakthrough and exhaustion of the active sites.

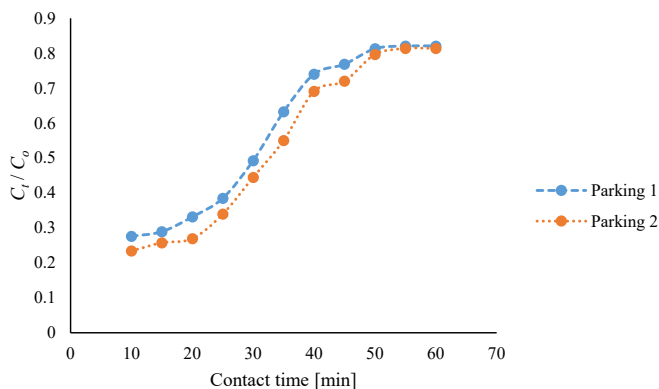


FIGURE 6. Effect of number of parking

Source: own work.

The increase in the number of beds leads to a greater amount of adsorbent within the adsorption column, providing more active sites for the removal of nitrate ions. Consequently, the overall removal efficiency of nitrate ions improves with the addition of multiple packing.

In summary, the introduction of multiple packing (beds) to the fixed bed column results in an enhanced performance and increased removal efficiency of nitrate ions. The inclusion of additional beds increases the available sorption sites and extends the service time until breakthrough and exhaustion of the active sites, leading to improved nitrate ion removal.

Column adsorption modeling

The experimental data obtained from the fixed bed adsorption experiment were analyzed using the Thomas, Adams–Bohart, and Yoon–Nelson kinetic models. The linear and non-linear forms of these models are presented in Table 1. The breakthrough behavior of the adsorption process was studied at different initial concentrations of nitrate ion, bed heights, and number of packing in the fixed bed column. The model parameters for each kinetic model were determined and are summarized in Table 5.

The Thomas model describes a rate-driving force and non-axial dispersion, assuming that internal and external diffusion are not the rate-controlling steps in the adsorption process. The q_o [$\text{mg}\cdot\text{g}^{-1}$] and K_{Tb} [$1\cdot\text{mg}^{-1}\cdot\text{min}^{-1}$] constants were obtained from the plots of $\ln\left(\frac{C_o}{C_t}\right)$ versus time (t). According to Table 5, an increase in the initial concentration of nitrate ions led to a decrease in q_o , which is contrary to the findings of Omitola et al. (2022). However, the value of K_{Tb} increased with increasing initial concentration, which aligns with the reports of Chowdury et al. (2013). It was observed that a notable correlation exist between the bed height and the Thomas model constant (K_{Tb}) wherein an increase in bed height from 3 cm to 7 cm coincides with a proportional rise in K_{Tb} . Conversely, an attendant decrease in the maximum adsorption capacity (q_o) is noted under the same conditions. This observation highlights the relationship between bed height and adsorption kinetics, wherein increased column height facilitates enhanced mass transfer. This consequently increase the rate of adsorption while potentially diluting the overall adsorption capacity. Moreover, the investigation reveals a noteworthy relationship between the number of packing units within the fixed-bed column and key adsorption parameters. Specifically, an increase in packing density correlates with an increase in q_o , indicative of a heightened capacity for adsorption. Interestingly, this trend is accompanied by a decline in K_{Tb} , suggesting an observable relationship between packing density and the rate of adsorption. Such observations underline the complex dynamics governing adsorption within fixed-bed columns, wherein

the arrangement and density of packing units exert discernible influences on adsorption kinetics and capacity. Furthermore, the robustness of the Thomas model in capturing the observed trends is highlighted by the high coefficient of determination (R^2) values obtained across varied experimental conditions (Abonyi et al., 2019; Obi et al., 2024). Particularly, R^2 values ranging from 0.677 to 0.807 for initial concentrations, 0.813 to 0.883 for fixed bed heights, and close to unity (ranging from 0.915 to 0.939) for the number of packing units. These results affirm the model's efficacy in accurately predicting adsorption behavior within the fixed-bed column. The implication of this findings challenges conventional notions regarding the rate-controlling steps in the adsorption process. This suggests that internal and external diffusion mechanisms, as posited by the Thomas model, may not singularly govern adsorption kinetics within the studied system. Rather, the observed relationship between bed height, packing density, and adsorption parameters highlights the need for a good understanding of the underlying mechanisms dictating adsorption behavior in fixed-bed columns, with potential implications for optimizing industrial-scale adsorption processes.

The Adams–Bohart model was analyzed by plotting $\ln\left(\frac{C_t}{C_o}\right)$ versus t . The slope and intercept of the plots were used to evaluate the N_o [$\text{mg}\cdot\text{l}^{-1}$], K_{AB} [$\text{l}\cdot\text{mg}^{-1}\cdot\text{min}^{-1}$], and R^2 parameters, which are also presented in Table 5. The study investigates the dynamic behavior of column adsorption using the Adams–Bohart model, a widely utilized framework for describing breakthrough curves in adsorption processes. The findings reveal distinct dependencies between key model parameters and experimental variables, shedding light on the intricate relationship within the system. In essence, this analysis demonstrates a discernible trend wherein the rate constant K_{AB} exhibits a decrease as the initial concentration of the adsorbate and the number of packing units are increased. Interestingly, a converse relationship emerges with respect to the bed height, showcasing an increase in K_{AB} as this parameter increase. This observation highlights the essential role bed height plays in modulating the kinetics of adsorption within the column system. Also, the characteristic parameter N_o indicative of the adsorption capacity of the column, exhibits a reduction with increasing initial concentration and bed height. Conversely, a rise is observed with an increasing number of packing units, indicating a pronounced effect of the latter on enhancing adsorption efficiency. Furthermore, the robustness of our model fitting is highlighted by the high R^2 (Abonyi et al., 2022; Ohale et al., 2023) values attained across varied experimental conditions. Specifically, the commendable R^2 values ranging from 0.669 to 0.802 for initial concentration, 0.809 to 0.880 for bed height, and 0.912 to 0.938 for

the number of packing units, affirm the reliability of the Adams–Bohart model in capturing the intricate dynamics of breakthrough curves.

The Yoon–Nelson model was utilized to determine the rate constant (K_{YN}) and the time required for 50% nitrate ion breakthrough (τ). The values of K_{YN} and τ were obtained from the slope and intercept of the Yoon–Nelson plot at different initial nitrate ion concentrations, bed heights, and number of packing, as presented in Table 5. Notably, K_{YN} exhibits a discernible trend, increasing with increased initial concentration and bed height, while witnessing a decline with an increasing number of packing units. This observation underlines the crucial influence of initial concentration and bed height on the kinetics of adsorption within the column, while highlighting the mitigating effect of packing density on the rate of adsorption.

TABLE 5. Column adsorption data

Effect of concentration									
Concentration [mg·l ⁻¹]	Thomas			Adams–Bohart			Yoon–Nelson		
	q_o [mg·g ⁻¹]	K_{Tb} [mg·l ⁻¹]	R^2	N_o [mg·l ⁻¹]	K_{AB} [l·mg ⁻¹ ·min ⁻¹]	R^2	K_{YN} [min ⁻¹]	τ [min]	R^2
100	449.936	0.0277	0.807	763.247	0.0280	0.802	0.0493	101.120	0.808
150	437.564	0.0281	0.677	665.400	0.0277	0.669	0.0572	89.033	0.671
200	395.836	0.0287	0.783	609.434	0.0275	0.776	0.0587	73.310	0.780
Heigh [cm]	Effect of bed height								
3	484.438	0.0249	0.883	855.780	0.0242	0.880	0.0426	113.280	0.889
5	443.304	0.0289	0.881	845.519	0.0251	0.878	0.0495	103.520	0.882
7	382.095	0.0370	0.813	673.366	0.0360	0.809	0.0632	89.477	0.817
Parking	Effect of number of parking in a column								
Parking 1	464.874	0.0278	0.915	820.203	0.0270	0.912	0.0475	108.820	0.917
Parking 2	564.344	0.0179	0.939	1 021.100	0.0170	0.938	0.0308	132.050	0.951

Source: own work.

Furthermore, the characteristic parameter τ , indicative of the mass transfer zone length, displays a contrasting pattern, diminishing with increasing initial concentration and bed height, but growing with an increasing number of packing units. The higher τ values are indicative of enhanced performance in the adsorption of nitrate ions from the aqueous solution, highlighting the efficacy of the column under varied experimental conditions. Moreover, the commendable R^2 values obtained for the Yoon–Nelson model across different experimental parameters further emphasized the model's predictive capability. With R^2 values ranging from 0.671 to

0.809 for initial concentration, 0.817 to 0.889 for bed height, and 0.917 to 0.951 for the number of packing units, the findings revealed the robustness of the model in capturing the intricate dynamics of breakthrough curves with high reliability.

Conclusions

The comprehensive analysis of the activated rice husk's surface chemistry through FTIR, SEM, SEM-EDS, and XRF techniques provided crucial insights into the nitrate ion adsorption process. The involvement of diverse functional groups, significant morphological alterations, and elemental compositions revealed the complex mechanisms underlying adsorption. Furthermore, the application of the Thomas, Adams–Bohart, and Yoon–Nelson models revealed distinct trends in adsorption behavior concerning initial concentration, bed height, and packing density. While the models demonstrated overall suitability, challenges were observed at higher initial concentrations, particularly evident with the Adams–Bohart model. Nonetheless, the consistent performance across varying parameters highlights the potential of these models for understanding and optimizing nitrate removal processes. Notably, the efficacy of double packing emerged as a promising strategy, offering enhanced performance compared to single packing configurations. This research provides significant insights into improving the removal of nitrates from water solutions, indicating practical applications for the development of effective adsorption systems. Future research could explore refining model parameters to address challenges at higher initial concentrations and further investigate the applicability of double packing configurations in larger-scale systems. Such advancements hold promise for addressing nitrate contamination challenges effectively.

Acknowledgments

We acknowledge the department of Chemical Engineering Nnamdi Azikiwe University, Awka for given us access to their laboratories for this research.

References

- Abonyi, M. N., Nwabanne, J. T., Igbonekwo, L. I., Ohale, P. E., Nwachukwu, J. O., Ezechukwu, C. M., & Ndibe, I. O. (2023). Parametric and kinetic study of hybrid dye uptake by activated mango seed endocar. *UNIZIK Journal of Engineering and Applied Sciences*, 2 (2), 285–300.

- Abonyi, M. N., Menkiti, M. C., Nwabanne, J. T., & Akomie G. K. (2022). Kinetic modeling and half-life study on bioremediation of crude oil dispersed by palm bunch enhanced stimulant, *Cleaner Chemical Engineering*, 2, 100031. <https://doi.org/10.1016/j.clce.2022.100031>
- Abonyi, M. N., Aniagor, C. O., Menkiti, M. C. (2019). Effective Dephenolation of Effluent from the Petroleum Industry Using Ionic-Liquid-Induced Hybrid Adsorbent. *Arabian Journal of Science and Engineering*, 44 (12), 10017–10029. <https://doi.org/10.1007/s13369-019-04000-8>
- Adeniyi, A., Ortiz, D. G., Bohatier, C. P., Mbakop, S., & Onyango, M. S. (2022). Preparation of nanofiltration membrane modified with sawdust-derived cellulose nanocrystals for removal of nitrate from drinking water. *Membranes*, 12 (7), 670. <https://doi.org/10.3390/membranes12070670>
- Battas, A., Gaidoumi, A. E., Ksakas, A., & Kherbeche, A. (2019). Adsorption study for the removal of nitrate from water using local clay. *The Scientific World Journal*, 2019, 9529618. <https://doi.org/10.1155/2019/9529618>
- Chen, W., Luan, J., Yu, X., & Wang, X. (2020). The preparation of novel mineral-based mesoporous microsphere by microencapsulation technology and its application in the adsorption of dye contaminants. *Water Science and Technology*, 81 (5), 985–999. <https://doi.org/10.2166/wst.2020.188>
- Chen, Y., Wu, ., Liu, C., Guo, L., Nie, J., & Ren, R. (2017). Continuous fixed-bed column study and adsorption modeling: Removal of arsenate and arsenite in aqueous solution by organic modified spent grains. *Polish Journal of Environmental Studies*, 26 (4), 1847–1854. <https://doi.org/10.15244/pjoes/68869>
- Chowdhury, Z. Z., Zain, S. M., Rashid, A. K., Rafique, R. F., & Khalid, K. (2013). Breakthrough curve analysis for column dynamics sorption of Mn (II) ions from wastewater by using Mangostana garcinia peel-based granular-activated carbon. *Journal of Chemistry*, 2013, 959761. <https://doi.org/10.1155/2013/959761>
- Daouda, K., Rahman, A. N., Valery, H. G., Nsami, N. J., Wahabou, A., & Mbadcam, K. J. (2018). Adsorption Equilibrium of Nitrates Ions onto Oil Palm Shells-based Activated Carbons. *Global Journal of Science Frontier Research: B Chemistry*, 18 (B2), 37–52.
- El Ouardi, M., Qourzal, S., Alahiane, S., Assabbane, A., & Douch, J. (2015). Effective removal of nitrates ions from aqueous solution using new clay as potential low-cost adsorbent. *Journal of Encapsulation and Adsorption Sciences*, 5 (4), 178–190. <http://dx.doi.org/10.4236/jeas.2015.54015>
- Foo, K. Y., & Hameed, B. H. (2012). Textural porosity, surface chemistry and adsorptive properties of durian shell derived activated carbon prepared by microwave assisted NaOH activation. *Chemical Engineering Journal*, 187, 53–62. <https://doi.org/10.1016/j.cej.2012.01.079>
- Hosseini, S. S., & Mahvi, A. H. (2018). Freezing process-a new approach for nitrate removal from drinking water. *Desalination and Water Treatment*, 130, 109–116. <https://doi.org/10.5004/dwt.2018.22963>
- Koter, S., Chojnowska, P., Szykiewicz, K., & Koter, I. (2015). Batch electro dialysis of ammonium nitrate and sulfate solutions. *Journal of Membrane Science*, 496, 219–228. <https://doi.org/10.1016/j.memsci.2015.08.064>

- Kumar, K. V., Valenzuela-Calahorro, C., Juarez, J. M., Molina-Sabio, M., Silvestre-Albero, J., & Rodriguez-Reinoso, F. (2010). Hybrid isotherms for adsorption and capillary condensation of N₂ at 77K on porous and non-porous materials. *Chemical Engineering Journal*, 162 (1), 424–429. <https://doi.org/10.1016/j.cej.2010.04.058>
- Li, Q., Li, X., Sun, J., Song, H., Wu, J., Wang, G., & Li, A. (2020). Removal of organic and inorganic matters from secondary effluent using resin adsorption and reuse of desorption eluate using ozone oxidation. *Chemosphere*, 251, 126442. <https://doi.org/10.1016/j.chemosphere.2020.126442>
- Li, Y., Wang, Y., Fu, L., Gao, Y., Zhao, H., & Zhou, W. (2017). Aerobic-heterotrophic nitrogen removal through nitrate reduction and ammonium assimilation by marine bacterium *Vibrio* sp. Y1-5. *Bioresource Technology*, 230, 103–111. <https://doi.org/10.1016/j.biortech.2017.01.049>
- Liu, X., He, C., Yu, X., Bai, Y., Ye, L., Wang, B., & Zhang, L. (2018). Net-like porous activated carbon materials from shrimp shell by solution-processed carbonization and H₃PO₄ activation for methylene blue adsorption. *Powder Technology*, 326, 181–189. <https://doi.org/10.1016/j.powtec.2017.12.034>
- Jahangiri-Rad, M., Jamshidi, A., Rafiee, M., & Nabizadeh, R. (2014). Adsorption performance of packed bed column for nitrate removal using PAN-oxime-nano Fe₂O₃. *Journal of Environmental Health Science and Engineering*, 12 (90), 1–5. <https://doi.org/10.1186/2052-336X-12-90>
- Jamka, Z. N., & Mohammed, W. T. (2023). Assessment of the feasibility of modified chitosan beads for the adsorption of nitrate from an aqueous solution. *Journal of Ecological Engineering*, 24 (2), 265–278. <https://doi.org/10.12911/22998993/156886>
- Jiaa, L., Jiangb, B., Huangb, F., & Hub, X. (2020). Adsorption and mechanism of nitrate from groundwater onto Si–Al porous clay mineral material as ceramic waste: characterization, kinetics, and adsorption isotherms, *Desalination and Water Treatment*, 202, 251–263. <https://doi.org/10.5004/dwt.2020.26184>
- Mondal, M. K. (2009). Removal of Pb (II) ions from aqueous solution using activated tea waste: Adsorption on a fixed-bed column. *Journal of Environmental Management*, 90 (11), 3266–3271. <https://doi.org/10.1016/j.jenvman.2009.05.025>
- Obi, C. C., Nwabanne, J. T., Igwegbe, C. A., Abonyi, M. N., Umembamalu, C. J., & Kamuche, T. T. (2024). Intelligent algorithms-aided modeling and optimization of the deturbidization of abattoir wastewater by electrocoagulation using aluminium electrodes. *Journal of Environmental Management*, 353, 120161. <https://doi.org/10.1016/j.jenvman.2024.120161>
- Omitola, O. B., Abonyi, M. N., Akpomie, K. G., & Dawodu, F. A. (2022). Adams-Bohart, Yoon-Nelson, and Thomas modeling of the fix-bed continuous column adsorption of amoxicillin onto silver nanoparticle-maize leaf composite. *Applied Water Science*, 12 (5), 94. <https://doi.org/10.1007/s13201-022-01624-4>
- Ohale, P. E., Chukwudi, K., Ndive, J. N., Michael, M. E., Abonyi, M. N., Chukwu, M. M., Obi, C. C., Onu, C. E., Igwegbe, C. A., & Azie, C. A., & Azie, C. O. (2023). Optimization of Fe₂O₃@BC-KC composite preparation for adsorption of Alizarin red S dye: Characterization, kinetics, equilibrium, and thermodynamic studies. *Results in Surfaces and Interfaces*, 13, 100157. <https://doi.org/10.1016/j.rsurfi.2023.100157>

- Quang, H. H. P., Phan, K. T., Ta, P. D. L., Dinh, N. T., Alomar, T. S., AlMasoud, N., Huang, C. W., Chauchan, A., & Nguyen, V. H. (2022). Nitrate removal from aqueous solution using watermelon rind derived biochar-supported ZrO₂ nanomaterial: Synthesis, characterization, and mechanism. *Arabian Journal of Chemistry*, 15 (10), 104106. <https://doi.org/10.1016/j.arabjc.2022.104106>
- Shelly, Y., Kuk, M., Menashe, O., Zeira, G., Azerrad, S., & Kurzbaum, E. (2021). Nitrate removal from a nitrate-rich reverse osmosis concentrate: Superior efficiency using the bioaugmentation of an *Acinetobacter* biofilm. *Journal of Water Process Engineering*, 44, 102425. <https://doi.org/10.1016/j.jwpe.2021.102425>
- Shi, Z., Zhang, Y., Zhou, J., Chen, M., & Wang, X. (2013). Biological removal of nitrate and ammonium under aerobic atmosphere by *Paracoccus versutus* LYM. *Bioresource Technology*, 148, 144–148. <https://doi.org/10.1016/j.biortech.2013.08.052>
- Swarup, B., & Umesh, M. (2015). Continuous fixed-bed column study and adsorption modeling: removal of lead ion from aqueous solution by charcoal originated from chemical carbonization of rubber wood sawdust. *Journal of Chemistry*, 2015, 907379.
- Taoufik, N., Elmchaouri, A., Korili, S. A., & Gil, A. (2020). Optimizing the removal of nitrate by adsorption onto activated carbon using response surface methodology based on the central composite design. *Journal of Applied Water Engineering and Research*, 8 (1), 66-77. <https://doi.org/10.1080/23249676.2020.1723446>
- Tejada-Tovar, C., Villabona-Ortíz, Á., & Gonzalez-Delgado, Á. D. (2021). Removal of nitrate ions using thermally and chemically modified bioadsorbents. *Applied Sciences*, 11 (18), 8455. <https://doi.org/10.3390/app11188455>
- Tong, X., Yang, Z., Xu, P., Li, Y., & Niu, X. (2017). Nitrate adsorption from aqueous solutions by calcined ternary Mg-Al-Fe hydrotalcite. *Water Science and Technology*, 75 (9), 2194-2203. <https://doi.org/10.2166/wst.2017.082>
- Tyagi, S., Rawtani, D., Khatri, N., & Tharmavaram, M. (2018). Strategies for nitrate removal from aqueous environment using nanotechnology: a review. *Journal of Water Process Engineering*, 21, 84–95. <https://doi.org/10.1016/j.jwpe.2017.12.005>
- Varsha, M., Kumar, P. S., & Rathi, B. S. (2022). A review on recent trends in the removal of emerging contaminants from aquatic environment using low-cost adsorbents. *Chemosphere*, 287, 132270. <https://doi.org/10.1016/j.chemosphere.2021.132270>
- Ward, M. H., Jones, R. R., Brender, J. D., De Kok, T. M., Weyer, P. J., Nolan, B. T., Villanueva, C. M., & Van Breda, S. G. (2018). Drinking water nitrate and human health: an updated review. *International Journal of Environmental Research and Public Health*, 15 (7), 1557. <https://doi.org/10.3390/ijerph15071557>
- Werth, C. J., Yan, C., & Troutman, J. P. (2020). Factors impeding replacement of ion exchange with (electro) catalytic treatment for nitrate removal from drinking water. *Acs Es&T Engineering*, 1 (1), 6–20. <https://doi.org/10.1021/acsestengg.0c00076>
- World Health Organization. (2017). *Guidelines for drinking-water quality, 4th edition, incorporating the 1st addendum*. WHO. <https://www.who.int/publications/i/item/9789241549950>

- Zhang, Y., Zheng, R., Zhao, J., Ma, F., Zhang, Y., & Meng, Q. (2014). Characterization of H₃PO₄-treated rice husk adsorbent and adsorption of copper (II) from aqueous solution. *BioMed Research International*, 2014, 496878. <https://doi.org/10.1155/2014/496878>
- Zheng, Y., & Wang, A. (2010). Nitrate adsorption using poly (dimethyl diallyl ammonium chloride)/polyacrylamide hydrogel. *Journal of Chemical & Engineering Data*, 55 (9), 3494-3500. <https://doi.org/10.1021/je100169r>

Summary

Adsorptive removal of a nitrate ion from the aqueous solution of sodium nitrate by application of double fixed-bed column. This study focuses on the removal of nitrate ions from aqueous solutions using rice husk activated carbon (RHAC). The RHAC was subjected to characterization via Fourier transform infrared (FTIR), scanning electron microscopy coupled with energy dispersive spectroscopy (SEM-EDS), and X-ray fluorescence (XRF) to ascertain its functional groups, surface morphology, and oxide/elemental composition, respectively. Batch experiments were conducted to assess the impact of nitrate concentration, bed height, and number of packing layers on removal efficiency. FTIR spectra revealed favorable sorption-related functional groups within RHAC, while SEM analysis indicated the presence of effective sorption sites on its surface. EDS analysis of the rice husk adsorbent before adsorption (RHBS) demonstrated a significant composition of Si (42.20%), O (35.30%), and Ca (12.33%). The batch study unveiled a concentration-dependent decrease in nitrate removal efficiency, alongside the enhanced performance with increased bed height and number of packing layers. Kinetic data fitting favored the Yoon–Nelson and Adams–Bohart models. Overall, RHAC exhibited efficient nitrate ion removal, with column performance notably improved by utilizing multiple packing layers. These results will enhance our understanding of the mechanisms involved in removing nitrate ions and highlight the potential effectiveness of RHAC, especially when utilized with multiple packing arrangements in column setups.